# Distributed Electric Spring Based Smart Thermal Loads for Overvoltage Prevention in LV Distributed Network Using Dynamic Consensus Approach

Tong Chen, *Student Member, IEEE*, Yu Zheng, *Member, IEEE*, Balarko Chaudhuri, *Senior Member, IEEE*, and S.Y.(Ron) Hui, *Fellow, IEEE*

***Abstract*--Overvoltage arising from reverse power flow in low-voltage (LV) distribution network caused by surplus roof-top photovoltaic (PV) energy generation is a major challenge in the emerging smart grid. This paper reports a study on the use of distributed thermal Smart Loads (SLs) for overvoltage prevention along a LV feeder. The basic principle involves the combined use of electric springs (ESs) and storage-type electric water heaters (EWHs) as distributed smart loads. Through distributed control, these smart loads play the important roles of mitigating reverse power flow problems and maintaining local mains voltage within the specified tolerance. Detailed modeling of the combined ES and EWH including their practical electrical and thermal capacities and constraints is adopted and optional distributed energy storage system (ESS) is also considered in the evaluation. Based on the Sha Lo Bay residential LV network in Lantau Island, Hong Kong, these case studies confirm the feasibility of the proposed approach for overvoltage prevention. The proposed distributed SLs-plus-ESS method is proved to be a cost-effective and environmental friendly way for overvoltage prevention in LV distributed network with high PV penetration.**

***Index Terms*--Smart grid, smart load, overvoltage problem, distribution networks, solar power**

## I. Nomenclature

| | |
|---|---|
| $t$ | Time variable. |
| $E_t$, $E_{1t}$, $E_{2t}$ | Thermal energy stored in the EWH, the upper layer of EWH, lower layer of the EWH at time *t*. |
| $L$ ,$L_{1t}$, $L_{2t}$ | Total volume of EWH and volume of upper layer and lower layer water in the EWH at time *t*. |
| $T_1$, $T_2$, $T_a$ | Inlet cold water temperature, hot water set temperature and ambient temperature. |
| $m$, $c$ | Density and specific heat capacity of water. |
| $U$ | Heat Loss coefficient of the EWH surfaces. |
| $E_{max}$, $E_{min}$, $E_a$ | Thermal energy stored in EWH when it is full of the water with pre-set hot water temperature, cold inlet water temperature and ambient temperature. |
| $P_t$, $\eta$ | Electric power of bottom heating unit at time *t* and efficiency of heating unit in EWH. |
| $P_{12t}$ | Thermal conduction between two water layer at time *t*. |
| $P_{a0}$, $P_{at}$ | Maximum heat loss and total Heat Loss from the EWH at time *t*. |
| $P_{a1t}$, $P_{a2t}$, | Heat Loss from the upper layer and lower layer water in the EWH at time *t*. |
| $SOTC_t$ | State of thermal charge in EWH at time *t*. |
| $W_t$ | Hot water draw at time *t*. |
| $V_s$, $V_n$, $V_{es}$ | Local bus voltage of SL, noncritical load voltage and the ES output voltage. |
| $Z$, $PF$, $I_n$ | Noncritical load impedance, power factor and current. |
| $P_{s0}$, $Q_{s0}$ | SL active and reactive power consumption when ES output voltage is zero. |
| $\Delta P_s$, $\Delta Q_s$ | SL active and reactive power consumption change with different ES output voltage. |
| $S_{es}$ | Apparent power of ES. |
| $V_0$ | Secondary voltage of the distribution transformer. |
| $V_i$ | Voltage at node-*i*. |
| $P_{Li}$, $Q_{Li}$ | Active and reactive power consumption at node-*i*. |
| $P_{si}$ | Active power injection by solar panels at node-*i*. |
| $Z_i$, $R_i$, $X_i$ | Line impedance, resistance and inductance between node-*i* and its upstream node. |
| $P_i$, $Q_i$, $S_i$ | Active, reactive and apparent power flow into node-*i*. |
| $a$ | Margin reserve for overvoltage prevention. |
| $b$ | Margin reserve for soft transition. |

## II. Introduction

FROM 2018, the Hong Kong SAR Government has allowed electricity consumers to apply to sell electricity back to the utility companies under a new 'feed-in tariff' scheme, hence opening a new era of "prosumers" in the Hong Kong electricity market. However, the injection of active power by distributed renewable power sources such as rooftop solar panels into low-voltage distribution networks could result in unacceptable overvoltage, which could reduce the lifetime of electric appliances and trigger overvoltage protection of solar panels. This problem has been highlighted by Math Bollen as one of the grand challenges in the emerging smart grid [1], and was later reported in Germany [2] and Hawaii [3] where renewable energy generation is substantial. Overvoltage problem could be particularly serious during noon time when the photovoltaic (PV) energy generation is high and load consumption is low in residential areas. With the surplus PV energy flowing in reverse direction, the voltage drop across the distribution line could result in high nodal voltage that exceeds +5% of the nominal mains voltage in the distribution network.

Conventional methods for mitigating the voltage rise issue include (i) active power curtailment of PV panels [4], (ii) reactive power control of PV inverter [5], (iii) distributed

energy storage installations [6], and (iv) a mixed approach of the above three methods [7]. However, active power curtailment may not be economical and will prolong payback time of PV facilities and the reactive control method could result in increased feeder losses [8]. The use of battery for energy storage is technically effective. But if new demand-side management techniques can be used to reduce the storage requirement, it would make the overall system more cost-effective. New methods for mitigating overvoltage in high PV penetration LV distribution network is therefore needed.

Demand-side management (DSM) is one effective solution to dealing with the disturbance caused by renewable energy technology. The use of domestic thermal loads, such as electric water heaters (EWHs) and air conditioners, was suggested by a US national laboratory in 2011 for providing regulation service [9]. The use of EWHs for providing regulation service was also reported in [10,11]. Distributed autonomous control of millions of thermostatic loads (fridges in particular) has also been discussed in [12] and [13].

Recently, electric spring (ES) technology [14,15] has been reported as a fast power-electronics-based DSM technology to reduce fluctuations in mains voltage and frequency caused by the intermittent nature of renewable energy sources. An ES can be used to turn a non-critical load (such as an EWH) into a smart load (SL) which consumes power adaptively to follow the fluctuating profile of the renewable power generation. The direct on-off control of EWHs evaluated in [9] requires an algorithm to coordinate the ***on-off*** control of 20,000 to 33,000 EWHs. Otherwise, a large power surge of load demand could result if all the EWHs are turned on or off simultaneously. On the other hand, the use of ES can provide a variable voltage to ***continuously operate*** the EWHs and ***adaptively control*** their power consumption to balance power supply and demand without shutting down the EWHs. Therefore, the ES approach will not cause noticeable user inconvenience and eliminates the possibility of on-off power surges. Moreover, since the surplus solar power is actually absorbed by the thermal loads, it is not abandoned or wasted.

This paper focuses on the novel research aspect of the use and control of distributed smart thermal loads for overvoltage prevention in the distribution line against reverse power flow caused by high penetration of distributed PV power generation. The new contributions include:

1) A two-layer integrated control scheme with the co-operation of smart thermal load and energy storage system (SL-plus-ESS) is proposed for overvoltage prevention in the LV residential network. The thermal smart load enjoys the priority to absorb the surplus PV power when overvoltage is about to happen. And the ESS serves as a backup and starts only when the capability of smart thermal load is not sufficient to handle the overvoltage issue.

2) The challenge of maximum-voltage-node uncertainty in the LV network with solar penetration is overcome by using dynamic consensus algorithm in this paper. Unlike the leader-following consensus, which has been used in previous literature, dynamic consensus algorithm used in this paper is a leaderless consensus control and thus overvoltage prevention for all the node in the network can be ensured without the previous empirical knowledge of where the maximum voltage may appear.

3) The case study based on the LV residential distribution line in Sha Lo Bay of the Lantau Island of Hong Kong verified the effectiveness of our proposal with the realistic models of storage-type EWH (including thermostat setting control and thermal capacity limits) and ES (including the real-time control and power rating limits). It shows that the SL-plus-ESS method can reduce the ESS (e.g. Battery) capacity requirement greatly compared with pure ESS method and thus save the installation cost (considering the batteries are more expensive than inverters).

## III. Model and Analysis of Electric Water Heater, Electric Spring and LV Distribution Network

### A. Dynamic Model of Storage-type Electric Water Heater

Traditionally, domestic EWHs have been used as "off-peak" electric loads to consume power after midnight in order to facilitate peak power shaving during daytime [16]. Full technical details and modeling of storage type EWHs can be found in [9].

As shown in Fig.1, the water tank is vertically divided into three layers: an upper layer with hot water, a lower layer with cold water and a mixing layer in between. The thickness of the mixing layer is assumed to be zero in this analysis. According to [9], the upper thermostat is for emergency use and thus is not considered in this paper. However, the bottom heating element is usually connected to an off-peak or timer-controlled electricity supply while the top heating element to a continuous supply [16]. So in this study, only the lower heating element is connected in series to the output voltage of an ES as shown in Fig.2(a). The inlet water temperature is assumed to be equal to the lower layer cold water temperature. ($T_{in}=T_1$).

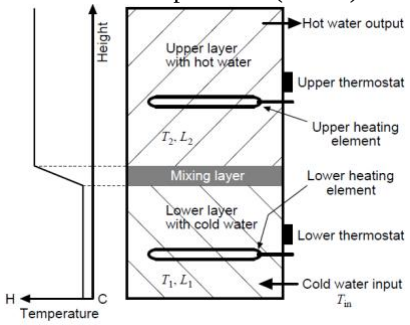


Fig. 1. Configuration and temperature profile of a large storage-type EWH [9]

Based on the analysis in [9], the thermal energy stored in the EWH is:

$$E_t = E_{1t} + E_{2t} = cmL_{1t}T_1 + cmL_{2t}T_2 \quad (1)$$

The heat loss from the EWH surface is:

$$P_{at} = UkL_{1t}(T_1 - T_a) + UkL_{2t}(T_2 - T_a) \quad (2)$$

$$P_{a0} = UkL(T_2 - T_a) \quad (3)$$

where $k$ is a coefficient relating the volume to the corresponding surface area. Define the state of thermal charge as:

$$SOTC_t = \frac{E_t - E_{\min}}{E_{\max} - E_{\min}} \quad (4)$$

where $E_{max}=cmLT_2$ and $E_{min}=cmLT_1$ are the thermal energy stored in the EWH when it is (i) full of hot water at the set temperature and (ii) full of inlet cold water, respectively. Now define $E_a=cmLT_a$ . Considering $L_{1t}+L_{2t}=L$, from (1)~(4):

$$P_{at} = P_{a0} \cdot \frac{E_t - E_a}{E_2 - E_a} \tag{5}$$

For $P_{a1t}+P_{a2t}=P_{at}$, considering the daily hot water draw, the water thermal energy change in the EWH can be written as:

$$\dot{E}_{1t} = cmW_t T_1 + \eta P_t - P_{a1t} + P_{12t} \tag{6}$$

$$\dot{E}_{2t} = -cmW_t T_2 - P_{a2t} - P_{12t} \tag{7}$$

$$\dot{E}_t = \dot{E}_{1t} + \dot{E}_{2t} = \eta P_t + cmW_t (T_1 - T_2) - P_{at} \tag{8}$$

Equation (8) shows the thermal dynamic model of EWH. The lower heating element of the EWH will be shut down when the temperature of its lower water layer reaches $T_2$. (i.e., $SOTC_t$ reaches 100%).

It worth noticing that, unlike those small EWHs with continuous electricity supply and are frequently on and off, the cold inlet water will not mix up with the existing hot water in the tank quickly in the large storage-type EWHs. The water in the big tank remains "thermally stratified" (with hot water at the top) and the hot water output would always be almost as hot as the water when the tank is fully heated. So there assume to be no noticeable hot water voltage drop (i.e. user inconvenience) when the SOTC value of the storage type EWH is still higher than 50%.

### *B. Electric Spring and Smart Load Capability*

A smart load (SL) in this paper is formed by connecting an electric spring (ES) in series with the lower heating element of the EWH (a noncritical load) as shown in Fig.2(a). An ES with back-to-back topology as shown in Fig.2 is adopted [17]. The control target of inverter-2 is to maintain a stable DC link voltage. The control schematic for inverter-2 can be found in [17] and will not be repeated here.

Inverter-1 is a voltage-controlled inverter which can generate a dynamic $V_{es}$ in order to regulate $V_s$ to its nominal value. In the process of regulating the local mains voltage, it provides a variable voltage $V_n$ for the heating element of EWH in order to modulate the power consumption of the EWH. When $V_{es}$ is generated to be in phase with $V_s$ as shown in Fig.2(b), the corresponding SL power consumption is reduced to support local mains voltage. When $V_{es}$ is generated to be out of phase with $V_s$ as shown in Fig.2(c), corresponding SL power consumption is boosted to suppress local mains voltage.

Based on this in-phase/out-of-phase control strategy of ES, the power change of SL with different ES output voltage can be expressed as:

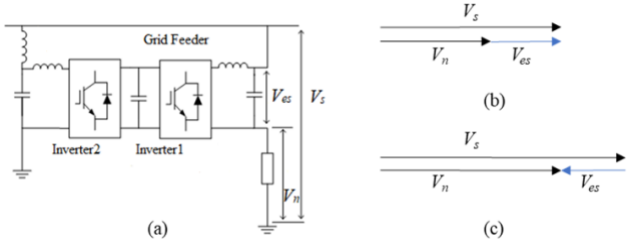


Fig. 2. ES-B2B based SL and its phasor diagram

$$\begin{cases} V_{n\_rms} = V_{s\_rms} - V_{es\_rms} \\ I_{n\_rms} = V_{n\_rms} / Z \\ P_{s0} = (V_{s\_rms}{}^2 / Z) \cdot (PF) \\ Q_{s0} = (V_{s\_rms}{}^2 / Z) \cdot \sqrt{1-(PF)^2} \\ \Delta P_s = V_{n\_rms} \cdot I_{n\_rms} \cdot (PF) - P_0 \\ \Delta Q_s = V_{s\_rms} I_{n\_rms} \sqrt{1-(PF)^2} - Q_0 \end{cases} \tag{9}$$

where the subscript *rms* refers to the root-mean-square (RMS) value of the variable. $\Delta P_s$ and $\Delta Q_s$ refer to the active and reactive power changes of the SL respectively under the same local mains voltage.

It is important to note that, for the back-to-back ES topology, the active power absorbed by inverter-1 is totally injected back into the power grid through inverter-2. ***So the active power consumption change on noncritical load is actually equal to the SL active power consumption change.*** So for a specific noncritical load (or SL) active power change $\Delta P_s$, corresponding $V_{es\_rms}$ and $\Delta Q_s$ can be calculated by using (9) as follows:

$$\begin{cases} V_{es\_rms} = V_{s\_rms} - \sqrt{V_{s\_rms}{}^2 + Z \cdot \Delta P_s / PF} \\ \Delta Q_s = V_{s\_rms} \cdot (\sqrt{V_{s\_rms}{}^2 + Z \cdot \Delta P_s / PF} - V_{s\_rms}) \cdot \sqrt{1-(PF)^2} / Z \end{cases} \tag{10}$$

Three realistic operation restrictions on ES and the normal noncritical load as proposed in [18] are considered in this study:

(i) ES voltage should be less than the local bus voltage.

(ii) Apparent power capacity of two inverters of ES with back-to-back topology is considered to be 20% of the nominal noncritical load power to ensure the size and the cost of the ES-B2B are economically reasonable.

(iii) The noncritical load (EWH heating element in this study) voltage should be within the range of 80%~120% of the nominal voltage.

The operation restrictions can be expressed in the per-unit system as follows:

$$\begin{cases} V_{es\_rms}{}^* < 1.0\text{p.u.} \\ S_{es}{}^* < 0.2\text{p.u.} \\ 0.8\text{p.u.} < V_{n\_rms}{}^* < 1.2\text{p.u.} \end{cases} \tag{11}$$

where the superscript * refers to the per-unit value of the variable. For individual noncritical loads, their respective rated apparent power values will be used as the bases for their per-unit apparent power values. The nominal mains voltage is used as the base for the per-unit voltage value.

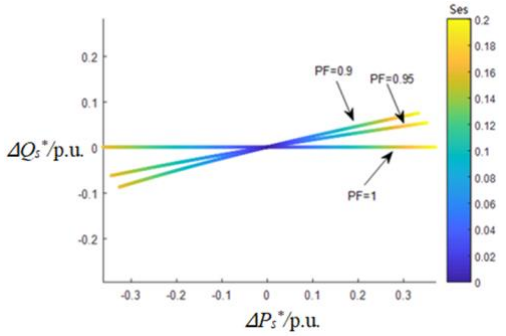


Fig. 3. $\Delta Q_s{}^*$-$\Delta P_s{}^*$ plot with different noncritical load power factor

The SL operating range (i.e. the variation range of active and reactive power) with the non-critical load power factor equal to 1.00, 0.95 and 0.90 are calculated and plotted in Fig.3. It can be seen from Fig.3 that the possible $\Delta P_{s*}$ range under the operation restriction (11) can reach at least +/-30% of its rated power consumption.

### C. Radial LV Distribution Feeder with High PV Penetration

Fig.4 shows a single-phase radial LV network with $n$ nodes. The apparent power transferred through LV line segment-$k$ is:

$$S_k = P_k + jQ_k = \sum_{i=k}^{n}(P_{Li} - P_{si}) + j\sum_{i=k}^{n} Q_{Li} \tag{12}$$

When this apparent power is transferred from node-($k$-1) to node-$k$, the line impedance between two adjacent nodes $Z_k = R_k + jX_k$ will cause a voltage drop. The voltage difference between $V_{(k-1)}$ and $V_k$ can be approximately expressed as (13) [19]

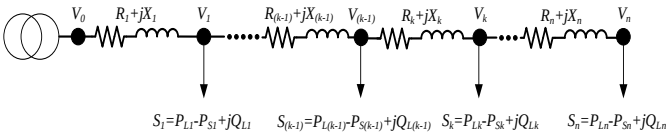


Fig. 4. Distributed line with high PV penetration

$$V_{(k-1)} - V_k = V_{dk} = \frac{R_k \cdot \sum_{i=k}^{n}(P_{Li} - P_{si}) + X_k \cdot \sum_{i=k}^{n} Q_{Li}}{V_k} \tag{13}$$

According to (13), with high PV penetration, a large value of the sum of $P_{si}$ may lead to $V_k > V_{(k-1)}$. If it is true for all the nodes in a feeder that the PV power generation at one node is larger than the load consumption at that same node, the maximum node voltage will appear at the end node of that feeder as shown in Fig.5(b). This is the case considered in many existed literature [20, 21]. However, considering the realistic situation that: (i) not all nodes are equipped with the PV panel; (ii) the PV power generation and load consumption may be different at different nodes at different times, the aforementioned assumption may not hold. So the maximum voltage ***may not always appear at the end node*** in reality. The situation that maximum node voltage appears at certain node in the middle of the LV feeder as shown in Fig.5(c) may happen. Moreover, the node with the highest nodal voltage may change with time since the variables in equation (13) are actually time variant.

In the cases that the maximum voltage does not appear at the end node, the application of leader-following consensus control [20, 21] for voltage regulation where the end node is chosen as the control leader cannot guarantee the node voltage of the whole network within the prescribed range. Thus dynamic consensus control is used in this paper instead.

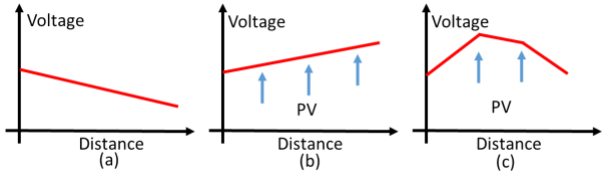


Fig.5 Possible voltage profile along a LV feeder

## IV. Distributed Smart Load and Energy Storage System for Overvoltage Prevention

Studies on the use of a single unit of ES has been reported in [18], [22] and [23]. This paper focuses on the use of dynamic consensus control on a group of distributed ESs for avoiding overvoltage situation arising from excessive PV power generation. Fig.6 shows the schematic of a distribution line feeding a number of households, each of which is represented by a module of a PV system, a SL (i.e. smart load), a critical load and an optional ESS. When the PV penetration rate is not too high, the power consumption boosting of SL group can compensate the surplus solar power generation during the noon time. In such cases, the backup ESS is not necessary. However, when the reverse power flow caused by PV panels cannot be fully absorbed by boosting the power consumption of SLs, the backup ESS (usually use lithium-ion battery) is needed at each node to absorb surplus PV active power. A sparse communication (Dashed red arrows in Fig.6) network is established to allow the bi-directional communication between two neighboring controllers. Dynamic consensus protocol [24] is used for feeder overvoltage prevention in this paper.

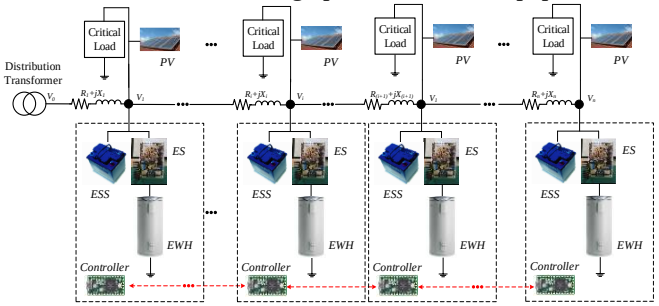


Fig. 6. Distributed SL-plus-ESS system in radial LV network with high PV penetration

### A. Overvoltage Prevention

Households are generally allowed to inject surplus solar power back to the grid on the condition that the local voltage meets the LV distribution system constraints. Fig.7 shows the control scheme for each local controller. The real-time local node voltage is sensed as $v_i$ and its RMS value $V_{i\_rms}$ is calculated. $V_{i\_rms}$ is subtracted from ($V_{\max}$ -$a$), of which the error ($e$) is fed into a proportional-integral (PI) compensator to generate $\Delta P_{si\_upper*}$ in per unit. The margin $a$ is reserved for the possible overshoot and oscillation caused by the slow dynamic of the PI control. The lower bound saturation of 0 p.u. of this PI compensator ensures zero PI output when the node RMS voltage is still within the permissible range. (i.e. lower than ($V_{\max}$ -$a$).) In this design, the PI output will restore to be zero automatically when the node voltage falls back to the preset permissible range.

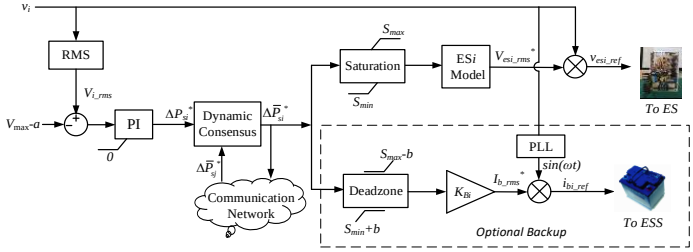


Fig. 7. Control scheme of each local controller

### B. Dynamic Consensus Protocol

In order to avoid different SLs competing with one another, consensus control is adopted to coordinate their operations. Since the location of the node with the highest voltage is uncertain (refer to Section III.C). With the prevalent leader-following consensus control [20, 21], even when the leader nodal voltage is controlled to be within the permissible voltage range, the maximum node voltage in the LV network may exceed the higher limit if it appears at the node other than the chosen leader load. In order to overcome this challenge, a dynamic consensus protocol is used to coordinate the distributed ES units in order to avoid overvoltage in the whole LV network in this paper.

As shown in Fig.7, $\Delta P_{si*}$ is updated with $\Delta\bar{P}_{si}^{\,*}$ according to the dynamic consensus protocol shown below [24]:

$$\Delta\bar{P}_{si}^{\,*}(t)=\Delta P_{si}^{\,*}(t)+\int_0^t\sum_{j=1}^{n}a_{ij}\cdot\left(\Delta\bar{P}_{sj}^{\,*}(\tau)-\Delta\bar{P}_{si}^{\,*}(\tau)\right)d\tau \qquad (14)$$

where $a_{ij}$ is the $(i,j)$ entry of adjacency matrix $A_n\in R_{n\times n}$. Setting $a_{ij}>0$ when ES$i$ can communicate with ES$j$. Otherwise, $a_{ij}=0$. The entries of the Laplacian matrix $L_n\in R_{n\times n}$ are defined as:

$$l_{ij}=\begin{cases}\sum_{i\neq j}a_{ij} & i=j\\ -a_{ij} & \text{otherwise}\end{cases} \qquad (15)$$

The global dynamics of the protocol (14) can be written as the matrix form as:

$$\Delta\dot{\bar{\mathrm{P}}}_{\mathrm{s}}^{\,*}=\Delta\dot{\mathrm{P}}_{\mathrm{s}}^{\,*}-L_n\Delta\bar{\mathrm{P}}_{\mathrm{s}}^{\,*} \qquad (16)$$

where $\Delta\bar{\mathrm{P}}_{\mathrm{s}}^{\,*}=\left[\Delta\bar{P}_{s1}^{\,*},\Delta\bar{P}_{s2}^{\,*},...,\Delta\bar{P}_{sn}^{\,*}\right]^{\mathrm{T}}$, $\Delta\mathrm{P}_{\mathrm{s}}^{\,*}=\left[\Delta P_{s1}^{\,*},\Delta P_{s2}^{\,*},...,\Delta P_{sn}^{\,*}\right]^{\mathrm{T}}$ are the information state vector and control variable vector respectively.

According to [25], (16) can be transferred into the frequency domain and written as:

$$\Delta\bar{\mathrm{P}}_{\mathrm{s}}^{\,*}(s)=s(sI_n+L_n)^{-1}\Delta\mathrm{P}_{\mathrm{s}}^{\,*}(s)=H(s)\Delta\mathrm{P}_{\mathrm{s}}^{\,*}(s) \qquad (17)$$

where $\Delta\bar{\mathrm{P}}_{\mathrm{s}}^{\,*}(s)$ and $\Delta\mathrm{P}_{\mathrm{s}}^{\,*}(s)$ are the Laplace transforms of $\Delta\bar{\mathrm{P}}_{\mathrm{s}}^{\,*}$ and $\Delta\mathrm{P}_{\mathrm{s}}^{\,*}$ respectively. $I_n\in R_{n\times n}$ is the identity matrix and $H(s)$ is the dynamic consensus transfer function. It has been demonstrated in [26] by using final value theorem that if the communication graph has a spanning tree with a balanced Laplacian matrix $L_n$,

$$\Delta\bar{\mathrm{P}}_{\mathrm{s}}^{\,*ss}=M_n\Delta\mathrm{P}_{\mathrm{s}}^{\,*}=\left\langle\Delta\mathrm{P}_{\mathrm{s}}^{\,*ss}\right\rangle\underline{1} \qquad (18)$$

where $M_n\in R_{n\times n}$ is the averaging matrix whose elements are all $1/n$. The symbol $\mathrm{x}_{ss}$ represents the steady-state value of vector $\mathrm{x}\in R_{n\times 1}$. And $\langle\mathrm{x}\rangle$ represents the average of all elements in the vector x. $\underline{1}\in R^{n\times 1}$ is a vector whose elements are all equal to one. That is to say that all $\Delta\bar{P}_{si}^{\,*}$, $i\in(1,2,\ldots,\mathrm{n})$, will ***converge to the global average value*** of $\Delta P_{si*}$ by using protocol (14).

Because the WiFi and Ultra-wideband (UWB) offer bandwidths up to 5 and 7.5GHz respectively [26], the dynamics of this consensus protocol in Fig.7 is considered to be much faster than that of PI controller of the power inverter. During the control process, ***once*** the voltage of an ***arbitrary*** node in the radial LV network first exceeds ($V_{\max}$ -$a$), its local PI compensator output $\Delta P_{si*}$ will first become nonzero. (The "first" also means this node is with the highest voltage in the network now) Through the dynamic consensus algorithm, the change of $\Delta P_{si*}$ propagates through the communication network with fast dynamics and affects all information states $\Delta\bar{P}_{si}^{\,*}$ ($i=1,2\ldots n$). All the $\Delta\bar{P}_{si}^{\,*}$ will converge to the global average value, which is also nonzero. In this way, the whole SL group will start to work in a coordinated way to suppress feeder nodal voltages once one nodal voltage in the network exceeds permissible limit.

### C. Cooperation of Smart Load and Energy Storage System

Using the updated $\Delta\bar{P}_{si}^{\,*}$ as the active power consumption change for the ES based SL in Fig.7, $V_{esi\_rms}$* can be calculated with equation (10). Upper and lower saturation limits are set to ensure the safe operation of SL. ($S_{\max}$ and $S_{\min}$ are stipulated to be +0.3p.u. and -0.3p.u., which are derived in Section IIB) Multiplying $V_{esi\_rms*}$ with the sensed real-time voltage $v_{si}$ signal, a time-variant reference $v_{esi\_ref}$ can be created as the control input for the inverter-1 of ES to perform sinusoidal PWM switching. The SPWM voltage waveform is then filtered by the LC filter to form the sinusoidal voltage $V_{es}$.

The dynamic consensus protocol converges the per-unit $\Delta\bar{P}_{si}^{\,*}$ values at different nodes to the same value. While the active power consumption of the EWH depends on the needs of individual household, it is varied by its ES with the same ratio. Consequently, consensus control enables a fair sharing of responsibility in overvoltage prevention in the event of reverse power flow. When the SL almost reaches its power limits (i.e. the EWH almost reaches its maximum permissible power output), a dead-zone section is used to ensure the startup of the ESS. The start and the end of the dead-zone are ($S_{\min}$ +$b$) and ($S_{\max}$ –$b$) respectively, where $b$ is the margin reserve for soft transition. Since all $\Delta\bar{P}_{si}^{\,*}$ values are identical, if one wants to achieve equally power input for all the distributed ESS units, the coefficient $K_{bi}$ should be set to be the same for all the nodes. However, if one wants the energy absorption of each ESS unit is with the same proportion of its capacity ($C_{essi}$), $K_{bi}/C_{essi}$ should be set identical for all the nodes. With the phase information obtained from the phase-lock-loop (PLL), a time-variant reference $i_{bi\_ref}$ , which is in-phase with the local node voltage, can be created as the control reference signal for the current-controlled grid-interface inverter of the ESS. And the excessive PV energy stored in ESS can be discharged to the critical load in the evening when the sunlight is absent.

## V. Case Study Based On Sha Luo Bay LV Network

To tackle the voltage problems caused by reverse power flow of distributed PV panels, the operating hours of these storage type EWHs will be shifted to the daytime instead of after midnight in this case study. This study is based on the assumption that all the domestic storage type EWHs are under a thermal load control program that makes them only operate in several continuous hours during noon time. Moreover, they are modified to be SLs with adaptive power consumption by using ES to further prevent the possible overvoltage problem brought out by excess solar power generation in LV network.

Fig.8 shows part of the radial distribution network at Sha Lo Bay in Lantau island of Hong Kong. The 11kV substation and a part of the 220V feeder network is included. The subfeeder-3 (highlighted in the red dashed rectangle) with 4 blocks is chosen as the test bench for evaluation. The four nodal voltages of this section of the LV feeder are measured by their local ESs installed at these 4 blocks as $V_1$,$V_2$,$V_3$ and $V_4$. The parameters of part of this distribution network can be obtained in [27] and shown in TABLE I. The turns ratio of the distribution transformer 3/1 is 11000:228.

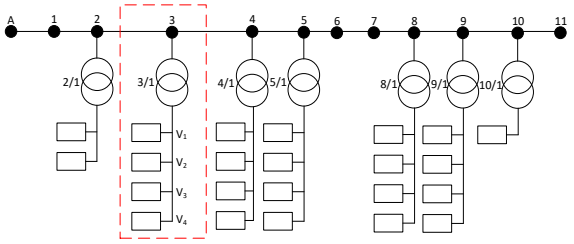


Fig.8. Sha Lo Bay LV Distribution Network[25]

TABLE I
DATA FOR SHA LO BAY NETWORK [25]

| From | To | Size | Distance(m) | R+jx(μΩ/m) |
|---|---|---|---|---|
| Sub A | 1 | 240 3/C | 600 | 98+j93 |
| 1 | 2 | 50 AAAC | 480 | 649+j335 |
| 2 | 3 | 50 AAAC | 285 | 649+j335 |
| 3 | 3/1 | 50 AAAC | 143 | 649+j335 |
| LV line between | Line | 4/0 AA | 27.9 | 302+j431 |
| two blocks | Neutral | 4/0 ACSR | 27.9 | 350+j461 |

It is assumed in the study that the loads of the 4 blocks in this study are identical and that each block consists of 2 households with their own ESSs, EWHs, PV panels and other critical loads. The typical daily hot water draw of a household, daily residential house load profile and PV daily output profile and can be found in [10], [28] and [29] respectively as shown in Fig.9. The EWH will continue operating once switched on and will shut down automatically when all the water in it reaches the preset temperature (i.e. SOTC=100%). The power rating of EWH is set at 1000W with 95% heating efficiency, the average power of residential load (excluding EWH) of one household during one day is assumed to be 2000W and the total hot water draw per day per household is assumed to be 190 liters [30]. The load power profile in the following section of this paper refers to the power consumption of other loads (critical loads) excluding the power for water heating [31]. The commercial EWH with a capacity of 315 liters for 3-4 people [16] is connected to an ES to form a SL, which is installed in each household. The inlet cold water is 10℃, ambient temperature is 20℃ and set temperature of all EWHs is 65℃. The other parameters of the EWH model can be found in [9]. Moreover, each household is equipped with the same backup ESS in case the SL capacity is not sufficient for overvoltage prevention. The overvoltage prevention margin $a$ in the control algorithm is set to be 0.005p.u. (i.e. 1.1V for 220V nominal voltage) in the control algorithm, so the maximum nodal voltage will not exceed 1.045p.u (under steady state).

Three case studies have been conducted to test the proposed SL-plus-ESS method for overvoltage prevention. Their conditions are listed as follows:

**Case-1:** Each household has installed a PV panel of a peak power rating of 4.5kW, a SL (comprising ES and EWH) and an ESS. Both of the SL and ESS are activated.

**Case-2:** The conditions are similar to those of Case-1, except that there are PV panels of peak power rating of 6kW in the first 3 blocks only.

**Case-3:** Repeat the study of Case-1, except that the ES is not activated.

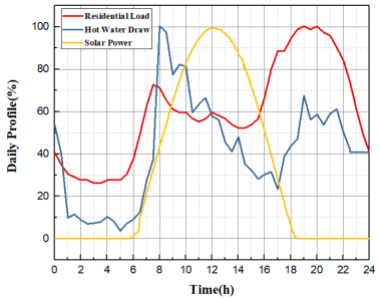


Fig. 9. Daily profiles of residential load, PV output and hot water draw

### A. Feeder Voltage Prevention

Assuming all the EWHs are turned on at 8:30am in this section. The SOTC defined in (4) is used as the charging state indicator of the EWH and the initial SOTC is assumed to be 84%. This assumption illustrates the worst-case scenario because all the EWHs will be turned on and shut down at the same time.

The simulation results for Case-1 and Case-2 (Fig.10(b) and Fig.11(b)) and their corresponding simulation results without the activation of proposed SL-plus-ESS method (Fig.10(a) and Fig.11(a)) are shown in Fig.10 and Fig.11. It can be seen that all of the 4 nodal voltages exceed 1.05p.u. around noontime in both cases. The maximum voltage appears at the end node (green curve for $V_4$ in Fig.10(a)) in Case-1. However, the maximum nodal voltage at noontime becomes $V_2$ (red curve for $V_2$ in Fig.11(a)) instead of $V_4$ in Case-2. The voltage profile along the LV feeder in Case-1 and Case-2 (when the overvoltage occurs) are demonstrated in Fig.12(a) and Fig.12(b) respectively. When the SL and ESS are activated, all the nodal voltages can be maintained below 1.05p.u and the maximum nodal voltage is controlled to be 1.045p.u. for both Case-1 and Case-2 as shown in Fig.10(b) and Fig.11(b).

It should be noted that Fig.10 and Fig.11 show the worst-case in the condition: (1) all the SLs are turned on and off at the same times; (2) the initial SOTC values and the hot water draw profile of all EWHs are identical. So there exist two large voltage transients because of the switching on and switching off of the EWHs. The following simulation results consider more general situations with different turn-on time and different initial SOTC values for the EWHs in different blocks.

### B. Load Shifting Effect of SL and Power Buffer Effect of ESS

In this section, the turn-on time of EWHs in the four blocks are randomized within the period of 8:00~9:00 with different initial SOTC values to mitigate the voltage transient mentioned before. Moreover, the discharge of ESS is also taken into consideration in this section. The ESSs of the four blocks are programmed to discharge with 1000W constant power at times

randomized over the time slot of 19:00~20:00 in order to avoid a large voltage transient.

The corresponding simulation results of Case-1 after the activation of the SL and ESS system are shown in Fig.13. The small voltage transients during 8:00~9:00 are caused by turning on EWHs. During 19:00~20:00 and 22:00~23:00, the small voltage transients are due to the start and end of the discharge of the ESS into the household loads. The rest of the small voltage changes are subject to the natural turn-off of the EWHs. It can be observed in Fig.13(a) that the maximum nodal voltage is kept at 1.045p.u. during 9:30~13:00 when reverse power flow could occur. The SOTC profiles of the EWHs of four blocks, the power profile for one block and the charging profile for one ESS are shown in Fig.13(b), Fig.13(c) and Fig.13(d) respectively.

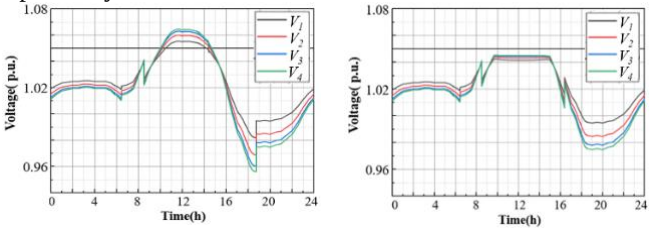


(a) SL and ESS are inactive (b) SL and ESS are active

Fig. 10 Nodal voltages with the Case-1 setup

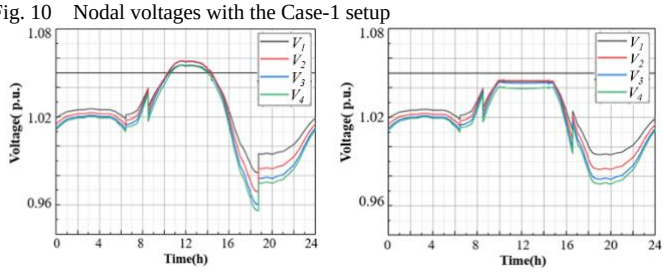


(a) SL and ESS are inactive (b) SL and ESS are active

Fig. 11 Nodal voltages with the Case-2 setup

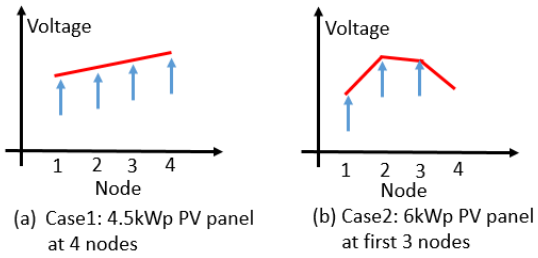


(a) Case1: 4.5kWp PV panel at 4 nodes (b) Case2: 6kWp PV panel at first 3 nodes

Fig. 12. The voltage profile along the LV feeder when the overvoltage occurs

The EWHs are turned on during 8:00~9:00 and shut down when their SOTC values reach 100% as shown in Fig.13(b). The SOTC values of the EWHs are always higher than 65%, indicating that the hot water supply for each household is sufficient in this case study. It can be observed in Fig.13(c) that: the EWH of this household is turned on at about 8:30am and its power consumption is boosted by the ES at around 9:35am to prevent the potential voltage rise caused by the increase of the PV output power. The EWH (or SL) nearly reaches its maximum power limits of 1300W at 10am and the backup ESS starts to absorb the surplus PV output energy and to limit the nodal voltages. The effectiveness of the control strategy proposed in section IV is well verified. The ESS starts working when the SL cannot fully buffer the PV power in order to avoid the overvoltage in the LV network. In the evening (19:00~22:00), the ESSs discharge their stored energy into the household load at 1000W as shown in Fig.13(c). Fig.13(d) shows the ESS charging and discharging phases. The maximum charging during one day is 3.15kWh per household. The stored energy in the ESS is consumed by the household loads in the evening to discharge the ESS.

In order to estimate the energy storage requirement of the ESS for overvoltage prevention *without* the effect of the ES, Case-3 has been conducted. The simulation results are shown in Fig.14. Fig.14(a) shows that the overvoltage can also be prevented. Without the ES to boost the power consumption up to 1.3 p.u. (i.e. 1300W), the EWH consumes the rated power of 1000W during the noon time as shown in Fig.14(c), resulting in longer heating time. Moreover, the ESS charging power has reached a higher level in Fig.14(c) (about 1300W) than that in Fig.13(c) (about 900W). Fig.14(d) shows that the ESS charging capacity in Case-3 is 4.8kWh per day, which is higher than 3.15kWh in Case-1. So the activation of the group of ESs in Case-1 allows more PV power to be absorbed by the EWHs and therefore reduces the total energy storage requirements in the distributed ESS systems.

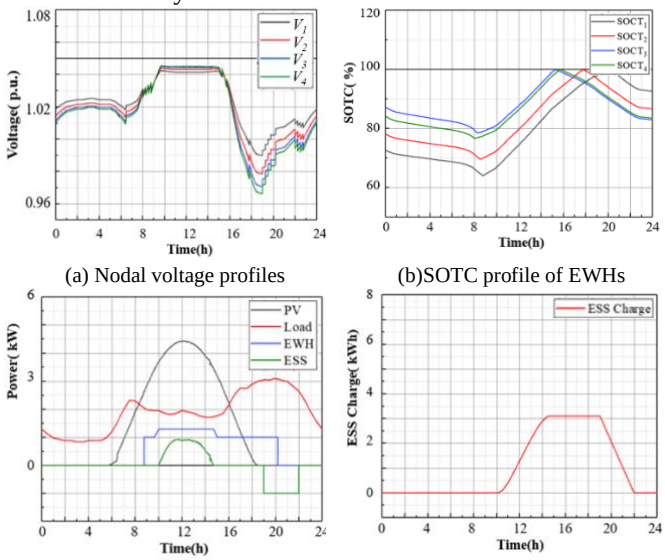


(a) Nodal voltage profiles (b)SOTC profile of EWHs

(c) Power profiles of one household (d)Charging and discharging profile of one ESS

Fig.13. Simulation results of Case-1 when SL-plus-ESS system is activated

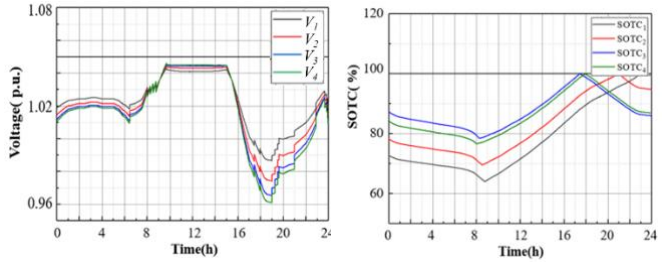


(a)Node voltage profiles (b)SOTC profile of EWHs

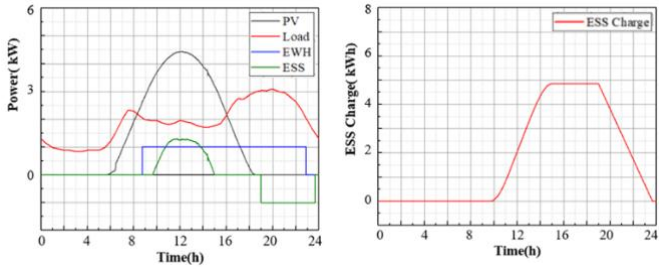


(c) Power profile of one household (d) Charging and discharging profile of one ESS

Fig. 14. Simulation results of case-3 with distributed pure ESS system when ES group is deactivated

Actually, the charging power reduction of ESS group is caused by the power shifting effect of thermal SL (or ES combined EWH). Fig.15 shows the power profile of the EWH and ESS in Case-1 and Case-3. The area in the "power versus time" diagram represents energy. When the ES is activated, it can boost the power consumption of the EWH by 30% during noon time. As a result, the EHW reaches it fully charged point and shuts down earlier. The ES effectively shifts the EWH energy consumption from $S_1$ to $S_2$ to buffer the surplus PV generation in the noontime as shown in Fig.15(a). At the same time, the energy absorbed by ESS is reduced by $S_3$ as shown in Fig.15(b). Approximately, $S_1$=$S_2$=$S_3$. This is the principle of how the proposed SL-plus-ESS method can reduce the distributed ESS capacity requirement for overvoltage prevention. Moreover, since the surplus PV power during the noontime is either stored in the thermal loads or stored in the ESS, no energy is wasted during this process.

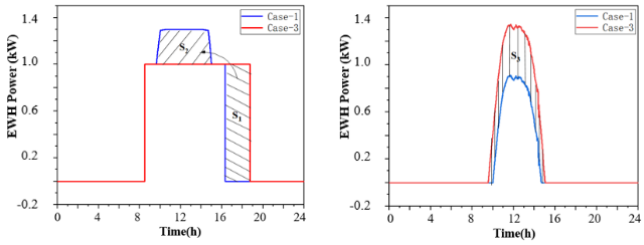


(a) Power profile of one EWH (b)Charging profile of one ESS

Fig. 15. Power profile caparison of case-1 and case-3

### C. Economic Benefit of Proposed SL-plus-ESS System

A rough economic analysis comparing the smart-load-plus-battery method and the pure battery method based on the Sha Lo Bay LV network is provided below to show the economic benefit of our proposed SL-plus-ESS system. It is shown that the cost reduction of Li-ion batteries when adopting our proposal is actually higher than the additional cost of inverters which are needed for Electric Springs.

An economic comparison between using our proposed method and the traditional pure batteries method is provided as follow: (Please note that the cost of ancillary converters for the battery system is neglected in our comparison, it will make the traditional method even more expensive when taking it into account)

The hardware cost for one household adopting the SL-plus-ESS system ($C_1$) can be described as:

$$C_1 = C_{ES\text{-}B2B} + C_{ESS} = 2 \times \alpha \times P_{rate} \times C_{inv} + (1+\beta) \times E_{charge1} \times C_{bat} \quad (19)$$

The hardware cost for the traditional distributed ESS system (C2) can be evaluated as:

$$C_2 = C_{ESS} = (1+\beta) \times E_{charge2} \times C_{bat} \quad (20)$$

where $C_{ES\text{-}B2B}$ and $C_{ESS}$ are ES-B2B cost and ESS cost respectively; $P_{rate}$ is the noncritical load rate power; $\alpha$ is the ES rate coefficient; $C_{inv}$ is the inverter price per kVA and $C_{bat}$ is the battery price per kWh, the multiplier 2 refers to the use of two inverters in the back-to-back inverter configuration; And $\beta$ is the battery reserve margin coefficient, $E_{charge1}$ and $E_{charge2}$ are the maximum electric charge of one ESS during one day with and without the use of the SL, respectively.

According to Section II, the power ratings of the two inverters in ES-B2B are designed 20% of the noncritical load rating ($\alpha$=0.2). The noncritical load in this study is EWH with 1000W power rating ($P_{rate}$ =1kW). According to recent survey (year 2018), the cost of standard inverter ($C_{inv}$) is $0.13 per watt [32] while the cost of the lithium-ion battery ($C_{bat}$) is $176 per kWh [33]. We assume the charge efficiency of the battery system is 92% and the allowable operating state-of-charge (SOC) range of the lithium-ion battery system is from 10% to 90% in this study. Considering a margin, the battery capacity is designed to be 2 times of the energy charge per day in this analysis (i.e. $\beta$=1). Thus, the cost of SL-plus-ESS system in each situation can be calculated.

TABLE II shows the $E_{charge1}$ and $E_{charge2}$ simulation results of the 5 cases with the peak power rating of PV panel installation per household ranges from 3kWp to 5kWp based on the Sha Lo Bay LV residential network. The respective economic costs for one household using these two strategies are calculated by (19) and (20) respectively.

TABLE II
ESS CHARGE AND ECONOMIC COST FOR ONE HOUSEHOLD
(WITH AN AVERAGE LOAD OF 3KW IN EACH HOUSEHOLD)

| PV peak power per house(kWp) | $E_{charge1}$(kWh) | $E_{charge2}$(kWh) | $C_1$($) | $C_2$($) |
|---|---|---|---|---|
| 3 | 0 | 0 | 52 | 0 |
| 3.5 | 0 | 0.38 | 52 | 134 |
| 4 | 1.06 | 2.41 | 425 | 848 |
| 4.5 | 3.15 | 4.80 | 1161 | 1690 |
| 5 | 5.89 | 7.84 | 2125 | 2760 |

It can be seen in TABLE II that the ESS charge and total cost is lower when we use the proposed SL-plus-ESS strategy when the PV power peak power is high. Fig.16 shows the economic cost of these two strategies. It can be seen that the more PV capacity exceeds the average household load consumption, the higher the cost required to prevent overvoltage arising from reverse power flow.

When each household is equipped with a 3.0kWp PV panel, there is no surplus PV power, but the hardware cost of SL-plus-ESS system is $52 considering the ES-B2B must be installed. When each household is equipped with a 3.5kWp PV panel (which is the case-1 setup in our paper), the hardware cost of or proposed method remains to be $52 because no extra battery is needed. In this case, $C_1$ is only 38.9% of the cost of the pure battery method ($C_2$=$134). When each household is equipped with a 4.5kWp PV panel (which is the case-1 setup in our paper), the hardware cost of SL-plus-ESS method is $1161

which is only 68.7% of the cost of the pure battery method ($1690). The reason why $C_1$ is lower than $C_2$ in this case is: the smart thermal load can absorb some surplus PV power into the hot water, resulting in a reduction of the Li-ion battery capacity needed; and the cost reduction of Li-ion batteries when adopting our proposal is actually higher than the additional cost of inverters which is needed for Electric Springs. It can also be observed in Fig.16 that with the endless increase of installed PV power rating per house, $C_1$ is less than $C_2$ while $C_1/C_2$ is tend to converge towards 1.0.

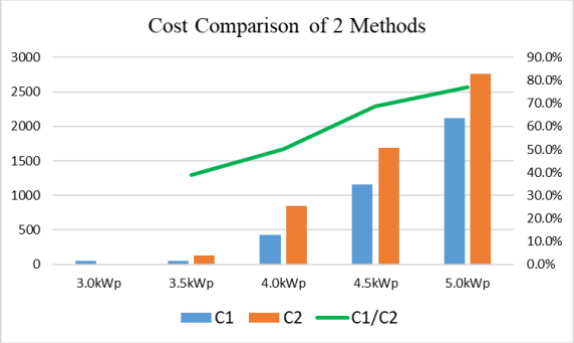


Fig. 16. Economic cost of ES-plus-ESS and pure ESS methods

## VI. Conclusion

Overvoltage problem in distribution lines arising from the reverse power flow of distributed rooftop PV panels has been previously identified as a grand challenge in the emerging smart grid. This paper presents the results of an investigation into the use of distributed smart loads for tackling this technical problem. With the aid of back-to-back electric spring circuits, traditional off-peak storage-type electric water heaters, previously designed for use after midnights, are modified into smart loads and used to absorb PV power during the day time. With dynamic consensus control, the study indicates that the smart loads can play an instrumental role in absorbing extra PV power in order to enable reverse power flow without having the local mains voltage exceeding the upper limit of the stipulated voltage value. The use of the proposed smart thermal loads also reduces the capacity requirements of the battery storage systems, thus potentially leading to reduced installation costs. Since the surplus solar power is actually stored in the thermal loads, it is not abandoned or wasted.

Further research should cover the climatic and economic aspects of the installations with the aim of evaluating the financial returns from a prosumer point of view.

## References


[1] Math Bollen, "The Smart Grid: Adapting the Power System to New Challenges", Chatper 1, Synthesis Lectures on Power Electronics, September 2011, Morgan & Claypool Publishers

[2] J. Von Appen, M. Braun, T. Stetz, K. Diwold, and D. Geibel, "Time in the sun: the challenge of high PV penetration in the German electric grid," *IEEE Power and Energy magazine*, vol. 11, no. 2, pp. 55-64, 2013.

[3] (2015). *Hawaiian grid requirements explained: overvoltage* [Online]. Available: http://www.smainverted.com/hawaiian-grid-requirements-explained-overvoltage/

[4] E. Demirok, D. Sera, R. Teodorescu, P. Rodriguez, and U. Borup, "Clustered PV inverters in LV networks: An overview of impacts and comparison of voltage control strategies," in *Electrical Power & Energy Conference (EPEC), 2009 IEEE*, 2009, pp. 1-6: IEEE.

[5] E. Demirok, D. Sera, R. Teodorescu, P. Rodriguez, and U. Borup, "Evaluation of the voltage support strategies for the low voltage grid connected PV generators," in *Energy Conversion Congress and Exposition (ECCE), 2010 IEEE*, 2010, pp. 710-717: IEEE.

[6] M. Alam, K. Muttaqi, and D. Sutanto, "Distributed energy storage for mitigation of voltage-rise impact caused by rooftop solar PV," in *Power and Energy Society General Meeting, 2012 IEEE*, 2012, pp. 1-8: IEEE.

[7] G. Mokhtari, A. Ghosh, G. Nourbakhsh, and G. Ledwich, "Smart robust resources control in LV network to deal with voltage rise issue," *IEEE Transactions on Sustainable Energy*, vol. 4, no. 4, pp. 1043-1050, 2013.

[8] P. M. Carvalho, P. F. Correia, and L. A. Ferreira, "Distributed reactive power generation control for voltage rise mitigation in distribution networks," *IEEE transactions on Power Systems*, vol. 23, no. 2, pp. 766-772, 2008.

[9] J. Kondoh, N. Lu, and D. J. Hammerstrom, "An evaluation of the water heater load potential for providing regulation service," in *Power and Energy Society General Meeting, 2011 IEEE*, 2011, pp. 1-8: IEEE.

[10] K. I. Elamari, "Using electric water heaters (EWHs) for power balancing and frequency control in PV-Diesel Hybrid mini-grids,", Master Thesis, Concordia University, 2011.

[11] K. Vanthournout, R. D'hulst, D. Geysen, and G. Jacobs, "A smart domestic hot water buffer," *IEEE Transactions on Smart grid*, vol. 3, no. 4, pp. 2121-2127, 2012.

[12] *Solar Inverter Costs and How to Choose the Right One* [Online]. Available: https://understandsolar.com/solar-inverter-costs/ [32] Tindemans, Trovato, Strbac, "Decentralized control of thermostatic loads for flexible demand response", IEEE Trans. Control Syst. Tech., vol. 23, no. 5, pp. 1685-1700, Sep. 2015

[13] Trovato, Martinez-Sanz, Chaudhuri, Strbac, "Advanced Control of Thermostatic Loads for Rapid Frequency Response in Great Britain," IEEE Trans. on Power Sys., vol. 32, no. 3, pp. 2106-2117, 2017

[14] S. Y. Hui, C. K. Lee, and F. F. Wu, "Electric springs—A new smart grid technology," *IEEE Transactions on Smart Grid*, vol. 3, no. 3, pp. 1552-1561, 2012.

[15] T. Chen, H. Liu, C. Lee and S. Y. R. Hui, "A Generalized Controller for Electric-Spring-Based Smart Load with Active and Reactive Power Compensation," *IEEE Journal of Emerging and Selected Topics in Power Electronics*, doi: 10.1109/JESTPE.2019.2908730

[16] *Off-peak, smart meters and time-of-use pricing* [Online]. Available: http://yourenergysavings.gov.au/information/peak-smart-meters-time-use-pricing

[17] S. Yan, C.K. Lee, T. Yang, K. Mok, S. Tan, B. Chaudhuri, S.Y.Hui, "Extending the Operating Range of Electric Spring Using Back-To-Back Converter: Hardware Implementation and Control," *IEEE Transactions on Power Electronics*, vol. 32, no. 7, pp. 5171-5179, 2017.

[18] Z. Akhtar, B. Chaudhuri, and S. Y. R. Hui, "Smart loads for voltage control in distribution networks," *IEEE Transactions on Smart Grid*, vol. 8, no. 2, pp. 937-946, 2017.

[19] P. Kundur, N. J. Balu, and M. G. Lauby, *Power system stability and control*. McGraw-hill New York, 1994.

[20] M. Alam, K. Muttaqi, and D. Sutanto, "Mitigation of rooftop solar PV impacts and evening peak support by managing available capacity of distributed energy storage systems," *IEEE Transactions on Power Systems*, vol. 28, no. 4, pp. 3874-3884, 2013.

[21] Y. Wang, K. Tan, X. Y. Peng, and P. L. So, "Coordinated control of distributed energy-storage systems for voltage regulation in distribution networks," *IEEE Transactions on Power Delivery*, vol. 31, no. 3, pp. 1132-1141, 2016.

[22] L. Liang, Y. Hou and D. J. Hill, "Enhancing Flexibility of an Islanded Microgrid With Electric Springs," in IEEE Transactions on Smart Grid, vol. 10, no. 1, pp. 899-909, Jan. 2019.

[23] C. K. Lee and S. Y. Ron. Hui, "Reduction of Energy Storage Requirements in Future Smart Grid Using Electric Springs," in IEEE Transactions on Smart Grid, vol. 4, no. 3, pp. 1282-1288, Sept. 2013

[24] D. P. Spanos, R. Olfati-Saber, and R. M. Murray, "Dynamic consensus on mobile networks," in *IFAC world congress*, 2005, pp. 1-6: Citeseer.

[25] V. Nasirian, S. Moayedi, A. Davoudi, and F. L. Lewis, "Distributed cooperative control of dc microgrids," *IEEE Transactions on Power Electronics*, vol. 30, no. 4, pp. 2288-2303, 2015.

[26] V. Nasirian, Q. Shafiee, J. M. Guerrero, F. L. Lewis, and A. Davoudi, "Droop-free distributed control for AC microgrids," *IEEE Transactions on Power Electronics*, vol. 31, no. 2, pp. 1600-1617, 2016.

[27] X. Luo, Z. Akhtar, C. K. Lee, B. Chaudhuri, S.-C. Tan, and S. Y. R. Hui, "Distributed voltage control with electric springs: Comparison with

STATCOM," *IEEE Transactions on Smart Grid*, vol. 6, no. 1, pp. 209-219, 2015.
[28] *Residential Energy Use (UK)* [Online]. Available: http://data.ukedc.rl.ac.uk/simplebrowse/edc/efficiency/residential
[29] *Solar Calendars* [Online]. Available: https://midcdmz.nrel.gov/apps/go2url.pl?site=SMUDA
[30] E. Fuentes, L. Arce, and J. Salom, "A review of domestic hot water consumption profiles for application in systems and buildings energy performance analysis," *Renewable and Sustainable Energy Reviews*, 2017.
[31] (2015, Sept). *Hong Kong Energy End-use Data2015* [Online]. Available: https://www.emsd.gov.hk/filemanager/en/content_762/HKEEUD2015.pdf
[32] 2018 Solar Panels Cost Per Watt Guide [Online]. Available: https://powerscout.com/site/2018-solar-panel-cost-per-watt
[33] A Behind the Scenes Take on Lithium-ion Battery Prices [Online]. Available: https://about.bnef.com/blog/behind-scenes-take-lithium-ion-battery-prices/

**Tong Chen** received the B.S. degree in electrical engineering from Xi'an Jiaotong University, Xi'an, China, in 2016. He is currently working toward the Ph.D. degree in electrical and electronics engineering with the University of Hong Kong, Hong Kong, China.

He is currently a visiting Ph.D. student with Imperial College London, London, U.K. His research interests include the stability and application of power electronics in power system and smart grid technology.

**Yu Zheng** (M'15) received the B.E. degree from Shanghai Jiao Tong University, China, in 2009, and the Ph.D. degree from the University of Newcastle, Australia, in 2015. He is currently a Senior Research Assistant with the University of Hong Kong, Hong Kong. He is also a Visiting Professor at the Changsha University of Science and Technology, Changsha, China. His research interests include power electronic applied in power systems, power system planning, and smart grid.

Y. Zheng is with the School of Electrical and Information Engineering, Changsha University of Science and Technology, Changsha 410004, China, and also with the Department of Electrical and Electronic Engineering, The University of Hong Kong, Hong Kong

**Balarko Chaudhuri** (M'06–SM'11) received the Ph.D. degree in Electrical and Electronic engineering from Imperial College London, London, U.K., in 2005 where he is presently a Reader in Power Systems. His research interest includes power systems dynamics and stability, grid integration of renewable energy, wide-area control through HVDC/FACTS and demand response. Dr Chaudhuri serves as an editor of the IEEE Transactions on Smart Grid and an associate editor of the IEEE Systems Journal and Elsevier Control Engineering Practice. He is a Fellow of the Institution of Engineering and Technology (IET).

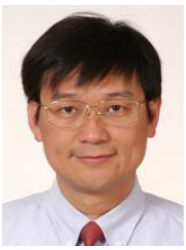

**S. Y. (Ron) Hui** (M'87-SM'94-F'03) received his BSc (Eng) Hons in Electrical and Electronic Engineering at the University of Birmingham in 1984 and a D.I.C. and PhD in Electrical Engineering at Imperial College London in 1987. Presently, he is a Chair Professor at the University of Hong Kong and Imperial College London. He received the IET Achievement Medal (The Crompton Medal) in 2010 and IEEE William E. Newell Power Electronics Award in 2015. He is a Fellow of the Australian Academy of Technological Sciences & Engineering (since 2010), US Academy of Inventors (since 2018) and the Royal Academy of Engineering, U.K. (since 2016).